Optical Coherence Tomography Layer Thickness Characterization of a Mock Artery during Angioplasty Balloon Deployment

Azarnoush, Hamed; Vergnole, Sébastien; Boulet, Benoît; Lamouche, Guy

Publisher's version / Version de l'éditeur:
https://doi.org/10.1117/12.877995
Proceedings of SPIE, 7963, 796328, 2011-03-03

Optical Coherence Tomography Layer Thickness Characterization of a Mock Artery during Angioplasty Balloon Deployment

Hamed Azarnoush[a,b], Sébastien Vergnole[a], Benoît Boulet[b], and Guy Lamouche[a]

[a]Industrial Materials Institute, National Research Council of Canada, Boucherville, QC, Canada
[b]Centre for Intelligent Machines, McGill University, Montréal, QC, Canada

ABSTRACT

Optical coherence tomography (OCT) is used to study the deformation of a mock artery in an angioplasty simulation setup. An OCT probe integrated in a balloon catheter provides intraluminal real-time images during balloon inflation. Swept-source OCT is used for imaging. A 4 mm semi-compliant polyurethane balloon is used for experiments. The balloon is inflated inside a custom-built multi-layer artery phantom. The phantom has three layers to mock artery layers, namely, intima, media and adventitia. Semi-automatic segmentation of phantom layers is performed to provide a detailed assessment of the phantom deformation at various inflation pressures. Characterization of luminal diameter and thickness of different layers of the mock artery is provided for various inflation pressures.

Keywords: optical coherence tomography, angioplasty, segmentation.

1. DESCRIPTION OF PURPOSE

Coronary angioplasty is performed on over 1 million patients, every year, in the US alone.[1] The large number of patients, suffering atherosclerosis and some drawbacks of angioplasty, e.g. restenosis,[2] underline the importance of further research to improve the outcome of the interventions. After the advent of the drug-eluting stents (DES), the restenosis rate was reduced. However, application of DES constitutes an improvement in the pharmacological approach rather than in the mechanical approach. Further analysis of mechanical behavior of the arteries may lead to improvement in the design of balloons or implants, such as stents. In the literature, this analysis has usually been performed in the form of uniaxial tensile tests of coronary strip specimens.[3] To our best knowledge no result has been published, presenting real-time monitoring of the interaction of the vessel wall and the balloon during inflation. One problem could be that intravascular ultrasound (IVUS) is the most available intravascular imaging technique which does not provide the desired resolution for this purpose. Another problem is the complexity of integrating an imaging probe inside a balloon catheter. Thus, addressing these problems is of high interest.

The paper is organized as follows. In section 2, we first describe our experimental setup for monitoring balloon inflation inside a multi-layer mock artery. We then describe the structure of IVOCT images and how different contours which delimit phantom layers are extracted. In section 3, we present characterization of luminal diameter and thicknesses of layers of the phantom during balloon inflation. The concluding remarks are included in section 4.

2. METHODS

2.1 Experimental setup

A custom-built swept-source OCT (SS-OCT)[4] system was used for imaging. We used a wavelength-swept laser source (Santec, HSL2000) operating with a sweep rate of 30 kHz and a sweep range of over 110 nm around 1.31 μm wavelength to provide a measured axial OCT resolution of about 12 μm in air. The SS-OCT system is configured as a Mach-Zehnder interferometer with balanced detection and is packaged as a mobile unit.

Figure 1. (a) OCT imaging balloon catheter (B: Balloon, F: ferrule, PS: polymer sheath, GRIN: gradient-index lens, LB: light beam, OF: optical fiber, PT: polymer tube, RAP: right-angle prism). (b) Photo of the OCT probe inside the inflated balloon

Figure 1 illustrates the composition of the OCT imaging balloon catheter. The details of this catheter were previously reported.[5] The OCT probe is composed of a single-mode fiber enclosed within a spiral metallic tube in the proximal region and within a polymer tube in the distal region. At the tip of the probe, the light is focused by a gradient index (GRIN) lens and redirected at 90° by a right-angle prism. The optical components are enclosed in a metallic ferrule. Rotation and translation are ensured by a custom pullback unit. The probe rotates in water within a polymer sheath (PS). The polymer sheath is used to protect the OCT probe and to prevent it from drifting away from the center of the balloon while rotating.

For our experiments, we used a 4 mm semi-compliant balloon from an extruded polyurethane tube. The balloon was inflated inside a custom-built multi-layer optical phantom.[6] The phantom is made of three layers with different optical scattering and optical attenuation properties. These layers simulate the layers of the coronary artery, namely, intima, media and adventitia. The phantom also has relevant mechanical properties in the small deformation regime.

2.2 IVOCT images

Figure 2 illustrates an acquired IVOCT image, in polar and Cartesian coordinates, when the balloon is inflated inside the phantom at a pressure of 2 atm. In Fig. 2(a) the lowest contour, corresponds to the prism surface. The polymer sheath and the balloon are represented each by two contours, corresponding to their inner and outer surfaces. The outer surface of the balloon together with the mock intima is viewed as one contour. The mock media and the mock adventitia can also be distinguished. In order to analyze the OCT image, we use the polar coordinate version of Fig. 2(a) where the horizontal and the vertical axes correspond to the probe rotation angle and the radial depth, respectively. The values on the primary axes (bottom and left) represent pixels. The values on the secondary (top and right) axes represent angle in degrees and the depth in millimeters in optical distance, i.e. the product of the geometrical distance and the refractive index. Each column in the image matrix represents depth scanning at a particular angle and is called an A-scan. A sample A-scan is depicted by a red line. The radial pixel size in our images is 8 μm in optical length. Imaging is performed at a rate of 20 frames per second.

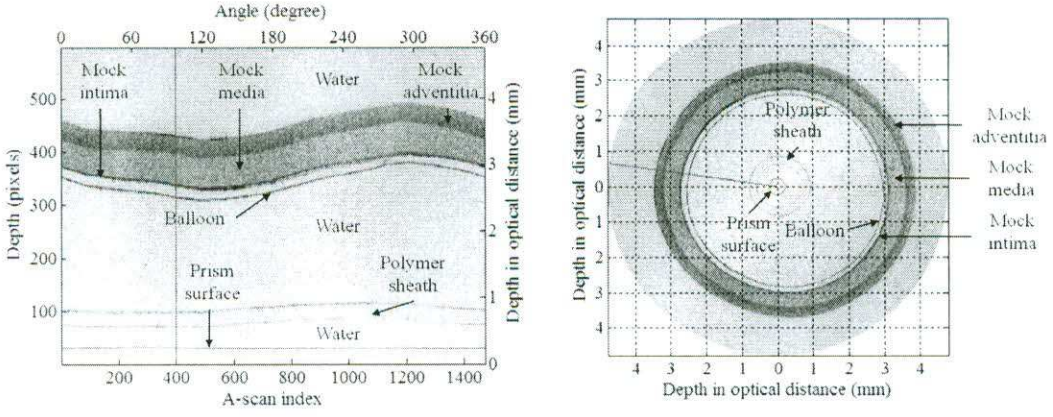

(a) Polar coordinates

(b) Cartesian coordinates

Figure 2. OCT image at an inflation pressure of 2 atm

2.3 Mock artery layer segmentation

In order to analyze the luminal diameter and the thicknesses of different layers of the phantom at different balloon inflation pressures, we perform a segmentation of the various contours of the IVOCT image. The image matrix in polar coordinates is used for this purpose. The intima is very thin and is detected as one contour. The thickness analysis is performed for the media and the adventitia. Referring to Fig. 2, for our diameter and thickness analysis, we extract:

- the contour, C_I, representing the intima,
- the contour, $C_{A/M}$, representing the interface between the adventitia and the media (A/M), and
- the contour, $C_{W/A}$, representing the interface between the water and the adventitia (W/A).

The thickness of the adventitia is calculated from the $C_{A/M}$ contour and the $C_{W/A}$ contour. The thickness of the media is calculated from the C_I contour and the $C_{A/M}$ contour.

For each contour, one node is detected per A-scan. A sequential approach is used to detect the contours. An arbitrary A-scan is chosen to start the contour detection. The contour's first node is detected on this A-scan. A neighborhood is defined around the depth of the detected node. This neighborhood serves as the search interval on the second A-scan. The second node of the contour is found in this neighborhood. This process continues until the last contour node is detected on the last A-scan.

The use of this sequential approach increases the speed of the algorithm. It also reduces the likelihood of generating outliers on the contours.

Figure 3 illustrates the A-scan which is depicted by a red line in Fig. 2. The contrast between grayscale intensities corresponding to the adventitia and the water regions appears as an edge on the A-scan. A similar edge is formed between the media and the adventitia regions. The former and the latter edges are in reversed directions. The intima on each A-scan is distinguished by a single peak. The contours $C_{W/A}$ and $C_{A/M}$ are detected as edges, while the contour C_I is detected as a ridge. First, $C_{W/A}$ and C_I are detected. Then, the search region on the starting A-scan is limited between the first nodes of $C_{W/A}$ and C_I to detect the first node of $C_{A/M}$. The sequential approach is used to follow the rest of $C_{A/M}$ nodes.

Detection of $C_{W/A}$:

A median filter with a coarse scale (order of 30 pixels) is applied to the first A-scan to eliminate single peaks. Then a gradient operation is performed. Considering the direction of the edge (high to low), the pixel that minimizes the gradient, estimates the location of the $C_{W/A}$ node on the first A-scan. Next, a neighborhood (10 pixels) around the detected pixel is defined. For a finer localization of the first $C_{W/A}$ node, cross-correlation with the rectangular edge filter, F_1 (Fig.4(a)), is performed. The pixel in the determined neighborhood that maximizes this cross-correlation is detected as the first $C_{W/A}$ node. The algorithm then proceeds to the second A-scan. On the second A-scan, the search is limited to a neighborhood (5 pixels) around the depth of the first contour node. By maximizing the cross-correlation with filter F_1 in the search interval, the second node of the contour is located. The same process is repeated until all A-scans are processed and all contour nodes are extracted.

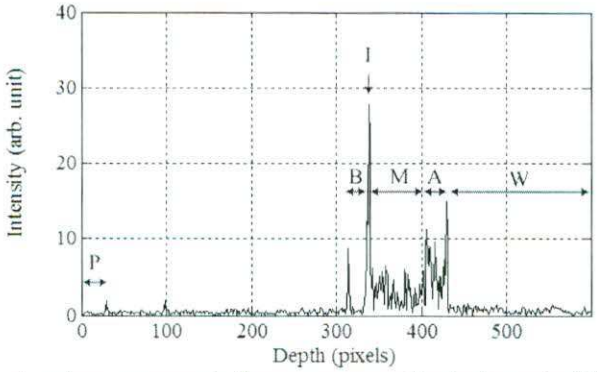

Figure 3. Identification of different regions on a sample A-scan corresponding to the water (W), the adventitia (A), the media (M), the intima (I), the balloon (B) and the prism (P)

(a) (b)

Figure 4. Filters used to extract contours

Detection of C_I:

As can be seen in Fig. 3, the locations of the two surfaces of the balloon are identified by two peaks. One corresponds to the inner surface of the balloon and the other corresponds to the contact between the outer surface of the balloon and the intima. The sets of two peaks, on the neighboring A-scans, when viewed alongside each other, form two ridges in the intensity image. These two ridges in proximity of each other demonstrate similar intensity characteristics and need to be distinguished. In our sequential contour detection, it is important to start detecting nodes on C_I and continue the detection on the same contour until all nodes are obtained. On the first A-scan, we detect a pixel between the two balloon surfaces and then proceed to obtaining the first C_I node. We exploit the fact that the balloon is viewed as two peaks on an A-scan. The pixel on the first A-scan that maximizes the cross-correlation of the A-scan with the filter, shown in Fig. 4(b), is identified as a pixel located between the two balloon surfaces. Here, the aim is to detect the C_I contour, which is the outer contour. Therefore, a search interval is placed on the outer side of the detected pixel. The size of the interval is chosen in a way that it includes the C_I node (20 pixels). In order to detect the C_I node, each node in the search interval is averaged with the nodes with the same depth from neighboring A-scans (5 A-scans from each side). The node that produces the largest average value is detected. This averaging operation is equivalent to cross-correlation with a horizontal line kernel.[7] A rotating kernel is not applied since the C_I contour does not have sharp variations across A-scans (Fig. 2(a)). On the second A-scan, a neighborhood (3 pixels on each side) is defined around the depth of the first contour node as the search interval. By using the same maximum average criterion in the search interval, the second node of the contour is located. The same process is repeated until all A-scans are processed and all contour nodes are detected.

Detection of $C_{A/M}$:

Once the $C_{W/A}$ and the C_I contours are detected, we proceed to detect the $C_{A/M}$ contour. The procedure will be similar to finding the $C_{W/A}$ contour, with the exception of reversing the direction of the edge filter, F_1. On the first A-scan, the search window is delimited by the corresponding nodes obtained for $C_{W/A}$ and C_I contours. When the first node of $C_{A/M}$ is obtained, on the second A-scan a smaller search interval (5 pixels on each side) is defined around the depth of the first detected node. The cross-correlation with the filter, obtained from reversing F_1, is used to find the second node. The process is repeated until all A-scans are processed and all contour nodes are detected.

3. RESULTS

Figure 5 presents segmentation of sample OCT images corresponding to the inflation of the balloon from a pressure of 0 atm to a pressure of 4 atm. At lower pressures, the balloon is not fully inflated. This causes the OCT images of the phantom to be distorted due to refraction of light in the balloon folding. This can be observed for inflation pressures of 0 atm and 1 atm in Fig. 5. When the balloon is fully inflated, the phantom can be viewed without such distortions. In our experiments the balloon was fully inflated at pressures of 2 atm and above. When there is not any distortion caused by balloon folding, our method for segmentation of the layers of the phantom is automatic. At lower inflation pressures (0 atm and 1 atm), the segmentation is semi-automatic. An operator first determines the range of A-scans that are not distorted. Automatic segmentation is then performed on all those A-scans. The segmentation for the distorted sections is obtained from interpolation between the automatically segmented sections.

Before extracting information from the contours, all values in optical length are converted to values in geometrical length. Figure 6(a) presents the estimated luminal diameter of the phantom at different balloon inflation pressures. The diameter is estimated based on the area of the lumen contour. First, the area of the detected C_I contour is

calculated. The estimated diameter for the lumen will be that of a circle with the same area. During the balloon inflation process, the estimated luminal diameter increases by 41 %.

Figure 6(b) presents a thickness analysis of the mock media, the mock adventitia, and the phantom (all layers) at different balloon inflation pressures. The figure provides the average and the standard deviation of the thicknesses obtained at various angular orientations. The average thicknesses of the mock media, the mock adventitia and the phantom decrease through the inflation process by 30 %, 20 %, and 27 %, respectively.

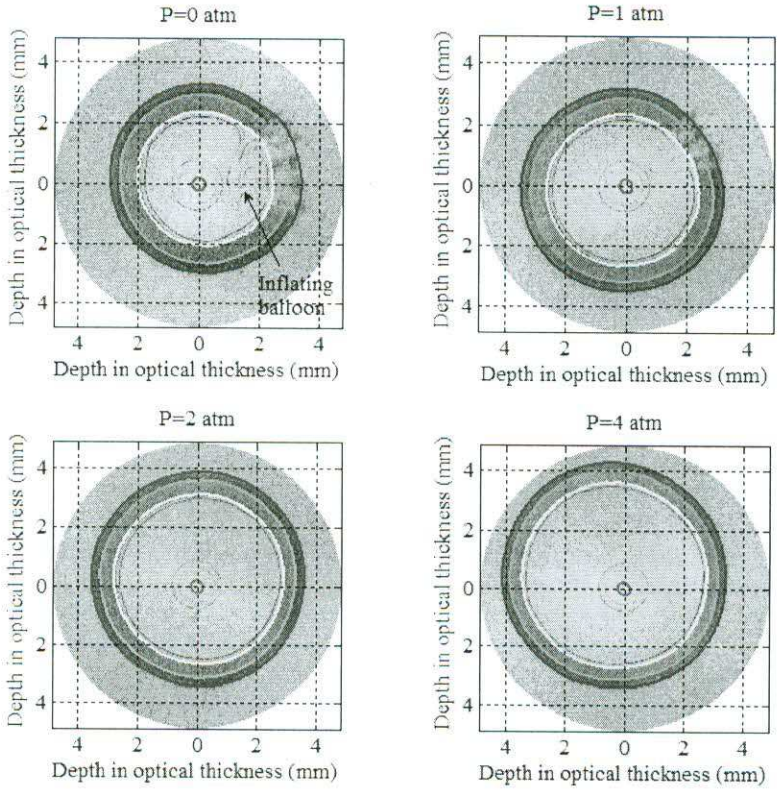

Figure 5. Segmented OCT images for various inflation pressures

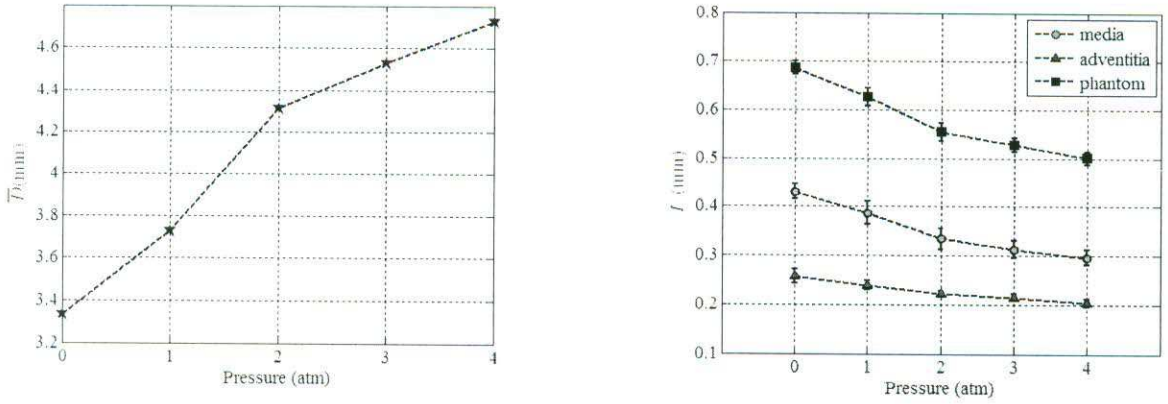

(a) (b)

Figure 6. Characterization of luminal diameter ($\overline{D}$) and layer thicknesses (T) for different balloon inflation pressures

4. CONCLUSIONS

In this paper, we proposed to monitor balloon inflation with IVOCT to assess tissue deformation. As an example, we presented characterization of luminal diameter and thickness of different layers of an artery phantom at different balloon inflation pressures. The presented approach, however, can go beyond thickness characterization and beyond phantoms. Therefore, a greater role is predicted for OCT in designing newer generations of percutaneous coronary intervention devices, or in clinical applications.

ACKNOWLEDGMENT

The authors would like to thank Christian de Grandpré for producing the balloon and for valuable technical support and Charles-Étienne Bisaillon for producing the phantom. We also acknowledge the financial support of the Genomics and Health Initiative of the National Research Council of Canada and the financial support of the Natural Sciences and Engineering Research Council of Canada.

REFERENCES

[1] Lloyd-Jones, D., et al., "Heart Disease and Stroke Statistics—2009 Update: a Report from the American Heart Association Statistics Committee and Stroke Statistics Subcommittee." Circulation, 119, e21-e181, (2009).

[2] Faxon, D. P., [Restenosis, a Guide to Therapy], Informa HealthCare, (2001).

[3] Holzapfel, G. A., Sommer, G., Gasser, C. T., and Regitnig, P., "Determination of layer-specific mechanical properties of human coronary arteries with nonatherosclerotic intimal thickening and related constitutive modeling," Am. J. Physiol. Heart Circ. Physiol., 289, H2048-H2058, (2005).

[4] Lamouche, G., Dufour, M., Hewko, M., Vergnole, S., Gauthier, B., Bisaillon, C-E., Monchalin, J-P., Sowa, M., "Intravascular optical coherence tomography on a beating heart model," Journal of Biomedical Optics 15, 046023-046027 (2010).

[5] Azarnoush, H., Vergnole, S., Bourezak, R., Boulet, B., and Lamouche, G., "Optical coherence tomography monitoring of angioplasty balloon inflation in a deployment tester," Rev. Sci. Instrum. 81 (8), 083101-8, (2010).

[6] Bisaillon, C.-E., Lanthier, M.-M., Dufour, M.L. and Lamouche, G., "Durable coronary artery phantoms for optical coherence tomography," Proc. SPIE 7161, 71612E1-10, (2010).

[7] Lee, Y., and Rhodes, W., "Nonlinear image processing by a rotating kernel transformation," Optics letters, 15, 1383-1385, (1990).